Semiconducting ZnSnxGe1−xN2 alloys prepared by reactive radio-frequency sputtering

Amanda M. Shing, Naomi C. Coronel, Nathan S. Lewis, and Harry A. Atwater

Citation: APL Materials **3**, 076104 (2015); doi: 10.1063/1.4927009
View online: http://dx.doi.org/10.1063/1.4927009
View Table of Contents: http://scitation.aip.org/content/aip/journal/aplmater/3/7?ver=pdfcov
Published by the AIP Publishing

Semiconducting $ZnSn_xGe_{1-x}N_2$ alloys prepared by reactive radio-frequency sputtering

Amanda M. Shing,[1] Naomi C. Coronel,[1] Nathan S. Lewis,[2] and Harry A. Atwater[3]
[1]*Department of Materials Science, California Institute of Technology, Pasadena, California 91125, USA*
[2]*Division of Chemistry and Chemical Engineering, California Institute of Technology, Pasadena, California 91125, USA*
[3]*Department of Applied Physics, California Institute of Technology, Pasadena, California 91125, USA*

(Received 1 June 2015; accepted 7 July 2015; published online 17 July 2015)

We report on the fabrication and structural and optoelectronic characterization of II-IV-nitride $ZnSn_xGe_{1-x}N_2$ thin-films. Three-target reactive radio-frequency sputtering was used to synthesize non-degenerately doped semiconducting alloys having <10% atomic composition (x = 0.025) of tin. These low-Sn alloys followed the structural and optoelectronic trends of the alloy series. Samples exhibited semiconducting properties, including optical band gaps and increasing in resistivities with temperature. Resistivity vs. temperature measurements indicated that low-Sn alloys were non-degenerately doped, whereas alloys with higher Sn content were degenerately doped. These films show potential for $ZnSn_xGe_{1-x}N_2$ as tunable semiconductor absorbers for possible use in photovoltaics, light-emitting diodes, or optical sensors. [http://dx.doi.org/10.1063/1.4927009]

$In_xGa_{1-x}N$ alloys are used in light-emitting diodes (LEDs) and sensors, where alloying enables tuning of the band-gap energy, $\mathbf{E}_g$, within the range set by the two binary compounds, InN ($\mathbf{E}_g$ = 0.69 eV) and GaN ($\mathbf{E}_g$ = 3.51 eV), allowing applications such as colored LEDs.[1] However, the large lattice mismatch between InN and GaN results in phase segregation for In-rich alloys, limiting the ability of the $In_xGa_{1-x}N$ alloys to cover the full visible spectrum.[2]

The Group II-IV nitrides are an emerging alloy series that is analogous to the well-characterized Group III-nitrides series with the Group III elements (In or Ga) replaced by a combination of a Group II element (Zn) and a Group IV element (Sn or Ge). Calculations performed using density functional theory (DFT) for the $ZnSn_xGe_{1-x}N_2$ alloys have predicted that the band gaps of the $ZnSn_xGe_{1-x}N_2$ alloy series will span the range of 1.4-3.1 eV, which includes the full visible spectrum, and suggest potential utility as photovoltaic absorber materials.[3] The calculated lattice parameters for $ZnSnN_2$ and $ZnGeN_2$ have a smaller mismatch (5%)[4] than the lattice parameters for InN and GaN (10%),[5,6] and experimentally, $ZnSn_xGe_{1-x}N_2$ alloys have demonstrated stability against phase segregation throughout the alloy series—a potentially significant advantage relative to $In_xGa_{1-x}N$ alloys.[3,7–9] $ZnSn_xGe_{1-x}N_2$ alloys also have the benefit of being composed of more abundant elements than $In_xGa_{1-x}N_2$ alloys, which may become either too difficult or too expensive to produce as In consumption increases. Specifically, the least abundant element in $ZnSn_xGe_{1-x}N_2$ alloys is Ge (1.5 mg kg^{-1}), which is about six times more abundant in the Earth's crust than In (0.25 mg kg^{-1}).[10]

Interest in the Zn IV nitride alloys first arose in the 1970s, when $ZnGeN_2$ was of interest as an alternative to GaN.[11,12] Fabrication of $ZnGeN_2$ has been attempted by various techniques including the vapor-phase reaction of Zn and Ge with NH_3,[13] high-pressure alloying of Ge_3N_4 with Zn[11] or Zn_3N_2,[14] metal-organic chemical-vapor deposition (MOCVD),[15] and sputter deposition.[16] These techniques have led to crystalline materials in the forms of high-pressure-formed pellets, micron-sized needles, and thin films. However, the properties of the materials have varied with the

synthetic technique and methods that produce $ZnGeN_2$ of sufficient electronic quality for use in devices require further development.

More recently, $ZnSnN_2$ has been synthesized by methods such as vapor-liquid-solid plasma-assisted growth[17] and molecular-beam epitaxy.[18,19] Reactive radio-frequency (RF) sputtering produces films that are more uniform than films fabricated using other methods. In addition, to date, all methods have reported $ZnSnN_2$ samples that exhibit majority carrier concentrations at or above degenerate doping levels.[18,19]

The preparation of sputtered $ZnSn_xGe_{1-x}N_2$ alloy films with compositions such that $0.025 < x < 1$ and the structural and optoelectronic properties of such films have been described previously.[9] Herein, we describe the preparation of samples with low-Sn content (less than 10% atomic concentration Sn, $x = 0.025$) and report on the structural and optoelectronic properties of these members of the $ZnSn_xGe_{1-x}N_2$ alloy series.

Thin-film samples were fabricated by reactive RF sputtering at a base pressure of 1×10^{-7} Torr from separate Zn, Sn, and Ge targets. Each target was 99.99+% pure, and the targets were held at varying RF powers during sputtering. Epitaxial-ready c-plane sapphire and GaN template substrates were rinsed with isopropanol, dried with a stream of nitrogen gas, and heated to 175 °C before deposition. During sputtering, the plasma in the chamber was maintained by a 1:3 argon:nitrogen gas-flow ratio at 3 mTorr pressure.

X-ray diffraction (XRD) patterns from the samples were collected and analyzed using a high-resolution X-ray diffractometer, employing Cu Kα radiation ($\lambda = 1.5418$ Å). The stoichiometry of the samples was measured using a scanning-electron microscope (SEM) equipped with an energy-dispersive spectrometer (EDS). Resistivities were measured using a four-point probe with W tips. Resistivities at varied temperatures were measured in a vacuum-sealed refrigerator with samples setup in the van der Pauw configuration. Carrier type was determined by the hot-probe technique, where samples were electrically contacted to a multimeter, while a heated (~150 C) probe touched the sample surface near one of the electrodes. The sign of the voltage output indicated the carrier type.

The dielectric functions were determined by spectroscopic ellipsometry, with the data modeled using a wavelength-by-wavelength layer on top of an alumina substrate layer.

Solid-state devices were characterized by two-point probe measurements under illumination, on a water-cooled stage that maintained constant temperatures. The samples were illuminated by chopped light from LEDs of various wavelengths.

Figure 1 shows the position of the $ZnSn_xGe_{1-x}N_2$ diffraction peak in the region of $33° < 2\theta < 34.5°$, indicating a linear shift in peak position with the Sn content of the films. Previous computational and experimental results support the assignments of an (002) orthorhombic $ZnSnN_2$ peak at $2\theta \approx 33°$ and of an (002) orthorhombic $ZnGeN_2$ peak at $2\theta \approx 34.5°$.[8,9] Vegard's law indicates that the corresponding peak for $ZnSn_xGe_{1-x}N_2$ alloys should lie between these two values. The (002) peak shifts linearly as the Sn content is varied for various $ZnSn_xGe_{1-x}N_2$ alloys having Sn atomic concentrations greater than 10%,[9] indicating that no phase segregation occurred for alloys with Sn concentrations greater than 10%. The linear shift with Sn content shown in Figure 1 indicates that phase segregation also does not occur for alloys with Sn atomic concentrations as low as 2%, thus extending the trend for the $ZnSn_xGe_{1-x}N_2$ alloy series. By using the full-width-half-max of the (002) peak in a Debye-Scherrer approximation, the film was inferred to consist of nanocrystalline grains that were tens of nm in size, which is consistent with the average grain size observed in SEM images of the surface of the films [Fig. 2].

The optical band gaps of the $ZnSn_xGe_{1-x}N_2$ alloys with <15% at. Sn were evaluated using spectroscopic ellipsometry. The optical constants n and k were obtained by fitting the polarization amplitude and shift. The absorption coefficients were calculated to be $>10^5$ cm^{-1}, indicating that the materials are well suited for use as thin-film light absorbers. Linear extrapolations from Tauc plots of the absorption coefficient squared versus energy showed that the low-Sn content alloys had direct band gaps ranging from ~2.2 eV to 2.7 eV. Figure 3 plots the measured optical band gaps versus % at. Sn. Samples with ≤7% at. Sn exhibited higher band gaps than samples having ≥10% at. Sn, consistent with previous observations.[9] The increase in band gap with decreasing Sn content has been attributed to tighter binding in which substitution of smaller germanium atoms opens the

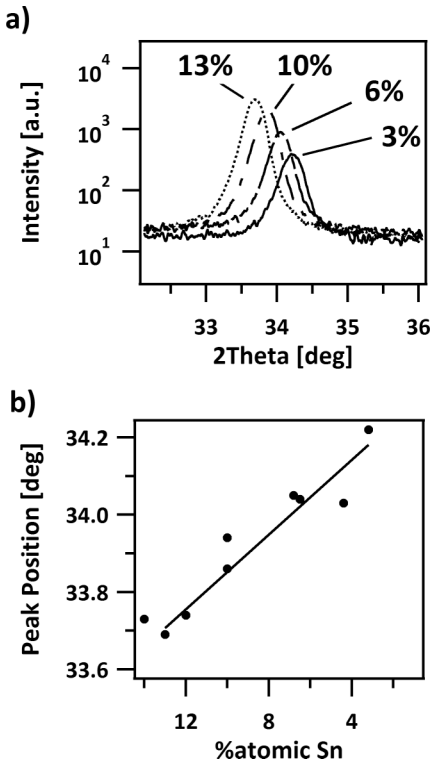

FIG. 1. (a) X-ray diffraction of shifting (002) $ZnSn_xGe_{1-x}N_2$ peak with varying Sn concentration. (b) Position of the 2θ peak versus Sn concentration showing the linear relationship between peak position and Sn composition.

band gap. The calculated partial density of states and band diagrams support this expectation for $ZnSnN_2$ and $ZnGeN_2$ (Ref. 3) in which the density of states in the conduction band contributed by Sn extends further into the band gap than do the states contributed by Ge.

Variations in the measured band gaps for a given composition may be attributed to the spread of samples, variations in strain, or to variations in substrates.

Figure 4 shows the dependence of the resistivity measured at room temperature using a four-point probe as a function of the Sn content the samples. $ZnSnN_2$ films exhibited resistivities of ~1 mΩ-cm. The resistivity increased exponentially with decreasing Sn concentration to $\sim 10^5$ Ω-cm for $ZnSn_xGe_{1-x}N_2$ alloys with <5% at. Sn. Thus, decreases in the Sn content produced increases in the resistivity of the $ZnSn_xGe_{1-x}N_2$ alloys. This behavior is consistent with previous work in which

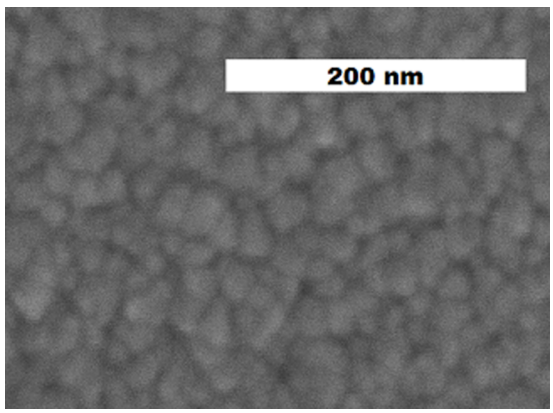

FIG. 2. Scanning electron micrograph of sputtered $ZnSn_xGe_{1-x}N_2$ surface. Surface features are <100 nm width.

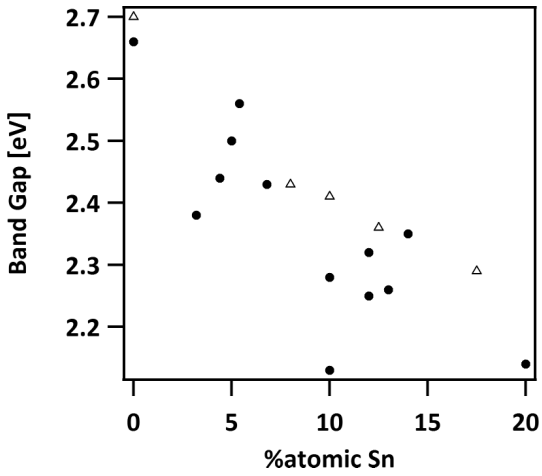

FIG. 3. Optical band gap versus percent atomic concentration of Sn. Measurements for samples prepared for this work are indicated by (●), while measurements reported in Ref. 9 for samples measured and modeled using the same methods employed herein are indicated by (△).

high carrier concentrations and low mobilities have been observed in $ZnSnN_2$ films and is consistent with the insulating character previously reported for sputtered $ZnGeN_2$ films.[15]

The exponential increase in resistivity with reduced Sn concentration can be attributed to an increase in the band gap and to a reduction in the number of thermally activated carriers in the conduction band of the alloys. Furthermore, substituting Ge for Sn may reduce the number of electrons available for conduction because Ge is more electronegative than Sn, hence Ge is a poorer electron donor than Sn. The exponential increase in resistivity with reduced Sn concentration may also reflect the location of the Fermi level ($\mathbf{E}_F$) with respect to the conduction-band energy ($\mathbf{E}_{cb}$) and with respect to excited carrier energies. If $\mathbf{E}_F$ were to remain the same while $\mathbf{E}_{cb}$ increases, then the resistivity would be expected to increase as additional Ge atoms are substituted for Sn.

Figure 5 shows the dependence of the resistivity on temperature for a sample with 5% at. Sn and for a sample with 16% at. Sn. Samples that had a low Sn concentration exhibited exponential increases in resistivity as the temperature decreased (Figure 5(a)), while samples having a higher Sn concentration exhibited a linear increase in resistivity as the temperature decreased (Figure 5(b)). Furthermore, the resistivity of the sample with low Sn concentration varied by two orders of magnitude over the 160-300 K temperature range, while the resistivity of the sample with the higher

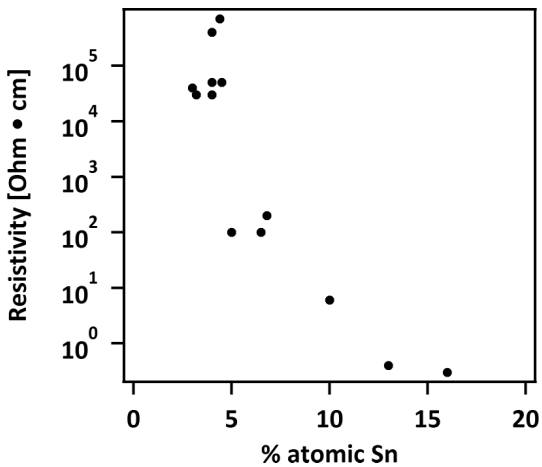

FIG. 4. Resistivity at 300 K of $ZnSn_xGe_{1-x}N_2$ thin films with varying Sn concentration. The resistivity increases exponentially with decreasing Sn content.

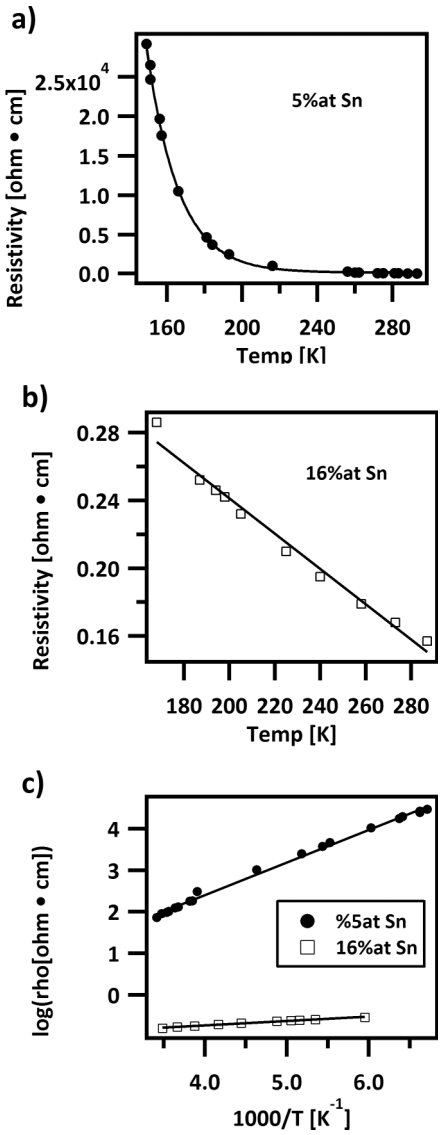

FIG. 5. Resistivity vs. temperature for samples with (a) 5% atomic concentration of Sn and (b) 16% atomic concentration of Sn. The samples exhibit behavior characteristic of semiconductors, with increasing resistivity over decreasing temperature. The change in resistivity over decreasing temperature indicate 16% at. Sn samples acting degenerately and 5% at. Sn samples acting non-degenerately. (c) Arrhenius plot (log of resistivity versus inverse temperature) for 5% at. and 16% at. samples. The greater slope of the 5% at. Sn trend line indicates a greater activation energy for thermalized carriers.

Sn concentration only varied by 100 mΩ-cm over the same temperature range. These results are characteristic of semiconductors for which the resistivity increases with decreasing temperature, as opposed to metals for which the resistivity decreases as the temperature decreases. Furthermore, the exponential resistivity-temperature trend observed for the low-Sn sample indicates that low-Sn samples act non-degenerately, differing from the remainder of the $ZnSn_xGe_{1-x}N_2$ alloys that have a higher Sn content. Thus, the electronic trends seen for the low-Sn quaternary alloys are distinctive within the $ZnSn_xGe_{1-x}N_2$ alloy series.

Although the charge-carrier mobility affects the resistivity, and although mobilities typically increase with decreased temperature due to reduced phonon scattering, the presence of grain boundaries and defects in a nanocrystalline material such as these sputtered $ZnSn_xGe_{1-x}N_2$ alloys likely dominates the mobility term and diminishes the change in mobility with temperature. Thus, the resistivity of these samples mainly reflects the carrier concentrations in the films.

The resistivity measurements were performed on samples of varying thickness, from 100 nm to 2 μm, and with varying input currents. The resistivities were on the same order of magnitude for samples having the same Sn tin content, regardless of the film thickness, and hence the measured resistivities are indicative primarily of bulk as opposed to surface carrier properties.

Figure 5(c) depicts an Arrhenius plot for the 5% at. Sn and 16% at. Sn samples. The slopes of the linearly fitted data yielded activation energies of 70 meV and 10 meV for the carriers in 5% at. Sn and 16% at. Sn samples, respectively. The decrease in activation energy as the Sn content increases agrees with the trends shown in Figures 4, 5(a) and 5(b) in which a higher conductivity is observed for the samples having higher Sn concentration, consistent with a reduced activation energy required for thermal excitation of carriers into the conduction band.

Hall measurements were not able to identify the carrier type in the films due to low mobilities (<10 $cm^2\ V^{-1}\ s^{-1}$). However, the hot probe technique performed on samples indicated n-type majority carriers.

Figure 6 shows two-point probe data that revealed a slow transient photoresponse, identified as persistent photoconductivity, which occurs in $ZnSn_xGe_{1-x}N_2$ alloys with $0 < x \leq 1$. The slow photoresponse can be attributed to free carriers interacting with molecular desorption of oxygen molecules, as in ZnO,[20,21] and as illustrated in Scheme 1. According to this mechanism, in the dark, an electron from the conduction band interacts with an oxygen molecule that adsorbs onto the surface. When the material is illuminated, an electron-hole pair is created and the hole recombines with the adsorbed-oxygen electron, leaving a remaining electron that increases the surface conductivity. When the optical excitation is terminated, molecular adsorption reoccurs, slowly capturing the free surface electrons,

$$\begin{aligned} &\text{Dark}: \quad e^- + O_2(g) \rightarrow O_2^-\ (\text{adsorbed}) \\ &\text{Light}: \quad h^+ + e^- + O_2^-(\text{adsorbed}) \rightarrow e^- + O_2\ (g). \end{aligned} \qquad \text{(Scheme 1)}$$

Persistent photoconductivity can also be attributed to a combination of shallow and deep traps, as in $SrTiO_3$, GaN, and $BiFeO_3$.[22–24] In this mechanism, a shallow trap constantly exchanges electrons with the conduction band, interfering with the generation and recombination of charge carriers at a deep trap. When illuminated, carriers generated from the deep trap will enter the conduction band states but begin to cycle into the shallow trap, causing a tailing onset for conductivity. When the optical excitation is terminated, electrons will begin to recombine. However, the shallow trap competes for electrons in the conduction band making it more difficult for electrons to reach the initial deep-trap state, resulting in persistent conductivity when in the dark. When in the conduction band, adsorbed oxygen may also play a role in addition to the shallow traps. Further

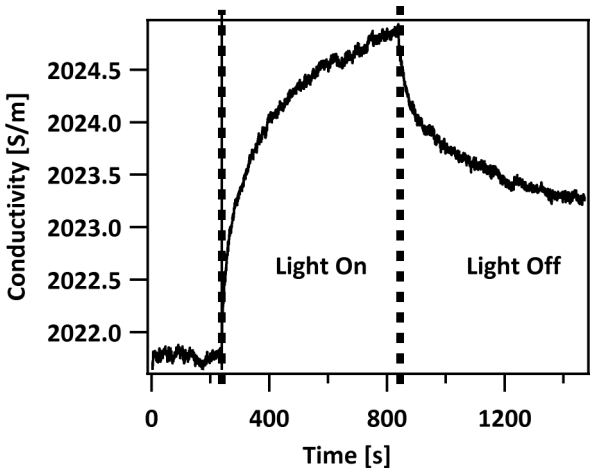

FIG. 6. Photoconductivity response of a solid-state $ZnSnN_2$ device at 5 V bias using white LED illumination at 30 mW/cm^2. A long response time is observed when the light is turned on and persistent photoconductivity is observed after turning the light off.

analysis of persistent photoconductivity in the $ZnSn_xGe_{1-x}N_2$ alloys, including investigations of defect-state densities, trap states, and molecular adsorption performed in a vacuum environment or with controlled gases, could indicate the potential contributions of these two persistent photoconductivity mechanisms.

In summary, the tunable band gaps across visible-light wavelengths provide an advantage for the potential device uses of the II-IV-nitrides relative to $In_xGa_{1-x}N_2$. $ZnSn_xGe_{1-x}N_2$ thin films that were fabricated using reactive RF sputtering and using three distinct targets and power supplies exhibited nanocrystalline grain sizes. Films with <10% at. Sn displayed non-degenerate electronic properties. For $0 \leq x \leq 1$, the $ZnSn_xGe_{1-x}N_2$ alloys do not phase segregate, and the band gaps of alloys with low Sn content are consistent with the overall bandgap trend for the entire alloy composition range. The resistivities of $ZnSnN_2$ are several milliohm-cm and resistivities of the $ZnSn_xGe_{1-x}N_2$ alloys increased exponentially with decreased Sn content, whereas sputtered $ZnGeN_2$ thin films exhibited insulating behavior. Electronic and optical measurements are consistent with the semiconducting properties of the $ZnSn_xGe_{1-x}N_2$ alloy series, in which low-Sn alloys have non-degenerately doped characteristics, and n-type majority carriers.

Devices exhibited persistent photoconductivity, and the observation of a photoresponse provides a positive outlook for development of $ZnSn_xGe_{1-x}N_2$ for photonic applications. Further development of crystallinity and defect density may enable $ZnSn_xGe_{1-x}N_2$ alloys to be useful as tunable materials in optoelectronic device applications.

The authors gratefully acknowledge support from the Dow Chemical Company under the earth-abundant semiconductor project. We also acknowledge the Joint Center for Artificial Photosynthesis and the Molecular Materials Research Center of the Beckman Institute at Caltech for instrument access.

[1] J. W. Shon, J. Ohta, K. Ueno, A. Kobayashi, and H. Fujioka, Sci. Rep. **4**, 5325 (2014).
[2] N. A. El-Masry, E. L. Piner, S. X. Liu, and S. M. Bedair, Appl. Phys. Lett. **72**(1), 40 (1998).
[3] A. Punya and W. R. L. Lambrecht, Phys. Rev. B **84**, 165204 (2011).
[4] A. Punya, T. R. Paudel, and W. R. L. Lambrecht, Phys. Status Solidi C **8**, 2492 (2011).
[5] S. Strite1 and H. Morkoç1, J. Vac. Sci. Technol., B: Microelectron. Nanometer Struct. **10**, 1237 (1992).
[6] A. F. Wright and J. S. Nelson, Phys. Rev. B **5**(12), 7866 (1995).
[7] K. T. Delaney, S. K. Shukla, and N. A. Spaldin, "First-Principles Theoretical Assessment of Earth-Abundant Nitrides for Photovoltaic and Optoelectronic Applications using Hybrid Density Functionals" (unpublished).
[8] L. Lahourcade, N. Coronel, K. Delaney, S. K. Shukla, N. A. Spaldin, and H. A. Atwater, Adv. Mater. **25**, 2562 (2013).
[9] N. Coronel, L. Lahourcade, K. T. Delaney, A. Shing, and H. A. Atwater, *2011 IEEE Photovoltaic Specialist Conference* (IEEE, 2011), p. 3204.
[10] *CRC Handbook of Chemistry and Physics, Internet Version*, 95th ed., edited by W. M. Haynes (CRC Press/Taylor and Francis, Florida, 2015), pp. 14–15.
[11] M. Maunaye and J. Lang, Mater. Res. Bull. **5**, 793 (1970).
[12] W. L. Larson, H. P. Maruska, and D. A. Stevenson, J. Elecrochem. Soc. **121**(12), 1673 (1974).
[13] K. Du, C. Bekele, C. C. Hayman, J. C. Angus, P. Pirouz, and K. Kash, J. Crystal Growth **310**, 1057 (2008).
[14] T. Endo, Y. Sato, E. Takizawa, and M. Shimada, J. Mater. Sci. Lett. **11**, 424 (1992).
[15] T. Misaki, A. Wakahara, H. Okada, and A. Yoshida, J. Crystal Growth **260**, 125 (2004).
[16] S. Kikawa and H. Morisaka, Solid State Commun. **112**(9), 513 (1999).
[17] P. Quayle, K. He, J. Shan, and K. Kash, MRS Commun. **3**, 135 (2013).
[18] N. Feldberg, J. D. Aldous, W. M. Linhart, L. J. Phillips, K. Durose, P. A. Stampe, R. J. Kennedy, D. O. Scanlon, G. Vardar, R. L. Field III, T. Y. Jen, R. S. Goldman, T. D. Veal, and S. M. Durbin, Appl. Phys. Lett. **103**, 042109 (2013).
[19] N. Feldberg, J. D. Aldous, P. A. Stampe, R. J. Kennedy, T. D. Veal, and S. M. Durbin, J. Electron. Mater. **43**(4), 884 (2014).
[20] P. Sharma, K. Sreenivas, and K. V. Rao, J. Appl. Phys. **93**(7), 3963 (2003).
[21] S. Kumar, V. Gupta, and K. Sreenivas, Nanotechnology **16**, 1167 (2005).
[22] A. Bhatnagar, Y. H. Kim, D. Hesse, and M. Alexe, Nanoletters **14**, 5224 (2014).
[23] M. Tarun, F. Selim, and M. McCluskey, Phys. Rev. Lett. **111**, 187403 (2013).
[24] C. H. Qiu and J. I. Pankove, Appl. Phys. Lett. **70**(15), 1983 (1997).